Journal of
Synchrotron Radiation

ISSN 0909-0495

Received 22 March 2010
Accepted 5 August 2010

Extended soft X-ray emission spectroscopy: quantitative assessment of emission intensities

Paul Pistor,[a]* Immo Kötschau,[a] Alex Grimm,[a] Christian Jung,[a] Iver Lauermann,[a] Martha Ch. Lux-Steiner[a,b] and Christian-H. Fischer[a,b]

[a]Helmholtz-Zentrum Berlin für Materialien und Energie GmbH, Glienicker Strasse 100, 14109 Berlin, Germany, and [b]Freie Universität Berlin, Fachbereich Physik, Arnimallee 14, 14195 Berlin, Germany. E-mail: paul.pistor@helmholtz-berlin.de

Soft X-ray emission spectroscopy (SXES) in the energy range between 150 eV and 1500 eV has typical attenuation lengths between tens and a few hundred nanometres. In this work the transmission of soft X-rays in synchrotron-based SXES has been quantitatively analysed using specially prepared layer samples. The possibility of extending the standard qualitative analysis of SXES by exploiting the information underlying the emission intensity was examined for thin layer structures. Three different experiment series were accomplished with model layer systems based on different sulfur-containing substrates: (i) MoS_2, (ii) $CuInS_2$, (iii) $Cu(In,Ga)(S,Se)_2$. The absorption of the S $L_{2,3}$ emission line by ZnO cover layers of up to 80 nm thickness was monitored and compared with theoretical expectations. By comparison with a reference intensity recorded from a bare substrate, the attenuation of the S $L_{2,3}$ emission could be used to accurately determine the ZnO overlayer thickness up to a critical thickness, depending on the set-up and the net S $L_{2,3}$ emission intensity. The results from these local energy-resolved spot measurements were compared with spatially resolved scans of the integral S $L_{2,3}$ emission intensity over areas of several mm^2. In the scan images the attenuation of the S $L_{2,3}$ emission intensity clearly reflects the local ZnO layer thickness. From the attenuation the ZnO layer thicknesses were calculated and compared with ellipsometric measurements and were found to be in excellent agreement. These results demonstrate the benefits of a quantitative analysis of SXES, making it an even more powerful tool for examining buried interfaces and for monitoring lateral inhomogeneities.

Keywords: soft X-ray emission spectroscopy; SXES; quantitative evaluation; film thickness; roughness; XES scan.

1. Introduction

Soft X-ray emission spectroscopy (SXES) is a well established tool for studying the electronic properties in solids and has already been used successfully for the characterization of thin film applications such as, for example, solar cells (Heske *et al.*, 1999, 2003; Weinhardt *et al.*, 2007; Rusu *et al.*, 2009). It offers several important useful features: (i) it is element-specific; (ii) the peak position and spectral shape can offer information on the local chemical environment of the probed element owing to the involvement of valence band states and the high-energy resolution; (iii) as a photon-in–photon-out process with an information depth of between several nanometres and a few hundred nanometres it is more bulk-sensitive compared with surface-sensitive X-ray methods such as photoelectron or Auger-electron spectroscopy and is therefore a complementary method. Its information depth makes it ideally suited for the investigation of thin-film structures and buried interfaces. The use of synchrotron light offers tunable excitation energy, very high photon fluxes and local excitation at a beam spot with submillimetre sizes.

Until now, attention has been drawn mainly to the qualitative interpretation of SXES data, examining chemical shifts or other changes in the shape of the recorded spectra, while the information underlying the relative intensity of emission lines is often not fully exploited. For XES with photon energies above 1500 eV [often called X-ray fluorescence analysis (XRF)], the quantitative evaluation of relative emission intensities is a standard procedure. However, here only the elemental composition can be derived since the resolution is usually not sufficient to reveal details of the local chemical environment of the analysed elements. Apart from compositional analysis, the determination of layer thickness is easily accomplished by XRF and even complex systems such as layer stacks can be evaluated using sophisticated modelling tools. This paper reports on an extension of these and similar

methods to the soft X-ray regime (100–1500 eV). Using well defined model systems we explore the determination of film thickness by comparison of relative emission intensities. An application of the more fundamental work presented here can be found in a contribution by Kötschau *et al.* (2007). In a previous paper we have quantified angle-resolved XES data (Mönig *et al.*, 2008).

2. Theory

The absorption of X-rays is governed by Beer's law,

$$I(x) = I_0 \exp(-\rho\mu x). \tag{1}$$

Here I_0 is the incident light intensity on a flat homogeneous sample of thickness x, and $I(x)$ is the attenuated X-ray intensity after passing through the sample. The specific absorption characteristics are determined by the (material- and wavelength-dependent) mass absorption coefficient μ and the material density ρ. In the following, Beer's law is applied to the geometry depicted in Fig. 1.

In the following a small volume within a sample is considered which is irradiated by X-rays. The SXES emission intensity of a given transition emerging from this volume as shown in Fig. 1 depends on a variety of factors as derived in the standard literature about XRF (Jenkins *et al.*, 1981; Tertian & Claissse, 1982). Namely, the emission intensity depends on the excitation intensity I_0, the attenuation of the exciting *and* emitted radiation and on the specific emissivity for the given emission line of the sample. The latter depends on factors such as the photo-ionization cross section, transition probability and fluorescence yield of the probed element and emission line.

For the depicted geometry (see Fig. 1) of a flat homogeneous sample under monochromatic excitation the formula for the emission intensity $\mathrm{d}I(x)$ of a thin layer element with thickness $\mathrm{d}x$ at sampling depth x is generally expressed as

$$\mathrm{d}I(x) = I_0 f \gamma B_1 \exp\left[\frac{-\rho\mu_{\mathrm{exc}} x}{\sin(\alpha)} + \frac{-\rho\mu_{\mathrm{emi}} x}{\sin(\beta)}\right] \mathrm{d}x, \tag{2}$$

where f is a geometrical factor determined by the given experimental set-up, B_1 is the fraction of exciting photons at x leading to photo-ionization of the considered core state within the layer element with thickness $\mathrm{d}x$, γ is the fraction of these photo-ionized states resulting in radiative emission of the specific emission line, ρ is the density of the sample, μ_{exc} and μ_{emi} are the specific mass absorption coefficients for the excitation and emission energy, respectively, and α and β are the incident and exit angle of the X-rays (see Fig. 1). In order to simplify, the effective mass absorption coefficient μ^* and the effective attenuation length α^*_{att} are introduced as follows,

$$\rho\mu^* = \frac{\rho\mu_{\mathrm{exc}}}{\sin(\alpha)} + \frac{\rho\mu_{\mathrm{emi}}}{\sin(\beta)} = \frac{1}{\alpha^*_{\mathrm{att}}}. \tag{3}$$

The total emission intensity of the sample is obtained by integration over the whole sample thickness. The total emission intensity increases proportionally as $1 - \exp(-\rho\mu^* d)$ with increasing thickness d of the emitting layer and saturates asymptotically for the idealized emission of an 'infinitely thick' sample. In practice, we will consider a sample as 'infinitely thick' if its emission intensity exceeds 99% of this saturation value. We call the saturated emission intensity of a specific emission line for an infinitely thick sample of a certain material its 'specific emissivity'. As this value is material specific and difficult to determine *a priori*, we rely in our study on a comparison with spectra of known reference samples from which the specific emissivity is determined experimentally. An emitting layer with thickness d and specific emissivity I_{ref} yields therefore an emission intensity of

$$I(d) = I_{\mathrm{ref}}\left[1 - \exp(-d/\alpha^*_{\mathrm{att}})\right]. \tag{4}$$

If the emitting layer is buried under a cover layer, of course both excitation and emissions are exponentially attenuated according to Beer's absorption law [equation (1)]. With the help of suitable reference spectra it is therefore possible to deduce information on the layer thicknesses of layered structures, either through the emission intensity of the layer itself or by the attenuation within the layer of a signal from below.

The accuracy of such a quantitative analysis is expected to be most reliable for very thin specimens and deteriorates as the emission intensities approach their saturation values. It needs to be mentioned that the above considerations hold for a flat homogeneous sample and difficulties arise with rough surfaces. Apart from problems in defining the layer thickness, shielding effects can lower the detected emission intensity in rough samples. In order to estimate errors based on surface roughness, a theoretical calculation of these effects based on a simple rectangular saw-tooth model was carried out. This calculation was based on models used by Borie for X-ray diffraction measurements (Borie, 1981), expanded to the case of different excitation and emission energies and absorption coefficients.

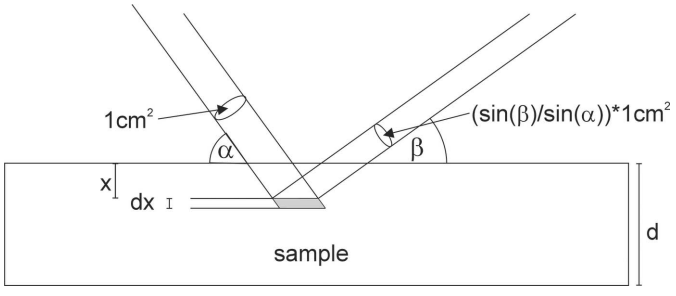

Figure 1
Sketch of the considered geometry for the SXES emission intensity.

3. Experimental

3.1. Sample preparation

In order to estimate the influence of the surface roughness, two plain thick Mo samples of known and distinct surface roughness were prepared. The surface roughness was initially determined by interference microscopy. Sample 1 is a sput-

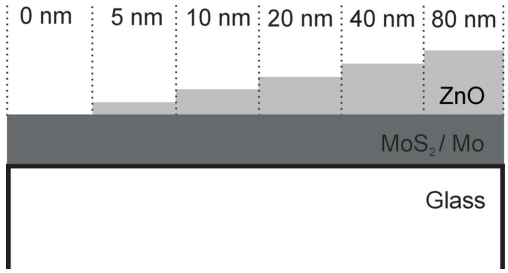

Figure 2
ZnO layers were deposited on a glass/Mo/MoS_2 substrate (with stepwise increasing ZnO layer thickness). The resulting staircase-like cross section is schematically illustrated (not to scale). The provided ZnO layer thicknesses are nominal values.

tered Mo layer on a glass substrate with a surface roughness (root mean square) of less than 1 nm. Sample 2 is a rolled Mo foil exhibiting a surface roughness of about 100 nm. From both samples Mo $M_{4,5}N_{2,3}$ emission spectra (attenuation length of 119 nm and 184 nm for excitation and emission, respectively) are recorded and evaluated as described above.

A model system was designed and fabricated consisting of a glass substrate covered by a sputtered Mo layer, which was sulfurized (resulting in a MoS_2 layer with a thickness of approximately 26 nm) and covered with ZnO layers (sample *A*). By subsequent masking and sputtering processes the ZnO cover layers were prepared in a staircase-like structure with five different steps of increasing ZnO layer thickness (Fig. 2 depicts a schematic cross section). The nominal thickness of the ZnO steps is 5 nm, 10 nm, 20 nm, 40 nm and 80 nm. One section of the glass/Mo/MoS_2 substrate was not covered by ZnO to enable the measurements of reference spectra on plain MoS_2. The thickness of the deposited ZnO layers was verified by ellipsometry measurements on this sample and revealed ZnO steps of 4.8 nm (± 0.3 nm), 10.9 nm (± 0.7nm), 20.4 nm (± 1.4 nm), 40 nm (± 3 nm) and 76 nm (± 6 nm).

Similar to the ZnO/MoS_2 system (sample *A*), two other model systems with a sulfur-containing substrate and an equivalent ZnO-staircase structure were fabricated. The substrate for sample *B* was a $CuInS_2$ (CIS) solar cell absorber from the HMI baseline after a KCN etching step [which removes the $Cu_{1-x}S$ secondary phase from the surface (Klaer *et al.*, 2003)]. Sample *C* consists of a Cu(In,Ga)$(S,Se)_2$ (CIGSSe) solar cell absorber (about 2 µm thick) from the pilot line of Shell Solar GmbH (Munich) covered in the same way as the other two samples with a ZnO structure.

Since the CIGSSe and CIS absorber layers exhibit a comparatively high surface roughness, precise ellipsometric measurements could not be performed on these samples. However, as the conditions for the ZnO sputter deposition were identical for all three samples and only initial variations in growth may contribute to differences in final film thickness, the final ZnO structure should be very similar in all three cases.

3.2. SXES set-up

All reported SXES measurements were recorded in the CISSY end-station at the high-flux beamline U41-PGM (Jung *et al.*, 2001) at Bessy II, Berlin, with a commercial XES300 spectrometer (Scienta Gamma Data) which is described in detail elsewhere (Nordgren & Guo, 2000). The detector of the spectrometer consists of a multi-channel plate in conjunction with a resistive anode assembly. The entrance slit, the grazing-incidence (focusing) diffraction grating and the detector satisfy the Rowland geometry. Samples were illuminated with synchrotron light under an angle of incidence α of 56° and measured under an exit angle β of 34° (to the surface). Fig. 3 shows a sketch of the basic set-up of the spectrometer including the last refocusing mirror unit at the end of the U41 beamline. The intensity of SXES emission is directly proportional to the intensity of incident excitation photons. Since the intensity of the synchrotron radiation decreases slowly between consecutive refills of the storage ring, the excitation intensity at the sample has to be monitored carefully during spectra acquisition. For a quantitative comparison, the recorded spectra are subsequently corrected for varying excitation conditions. The last refocusing mirror unit of beamline U41-PGM allows the incident excitation intensity to be monitored by measuring the photocurrent of the isolated gold-coated refocusing mirror. Since only fixed apertures limit the emerging beam from this mirror to the sample's surface, the measured photocurrent can be used as a direct monitor of the excitation intensity at the sample. In practice, the photocurrent of the refocusing mirror is permanently recorded during all SXES measurements. That way, measured SXES emission intensities can be normalized *via* the recorded mirror photocurrent to standardized excitation conditions.

There are, in principle, two modes available at the CISSY end-station for recording the SXES emission. In the first mode a full energy-dispersive spectrum is acquired over a time

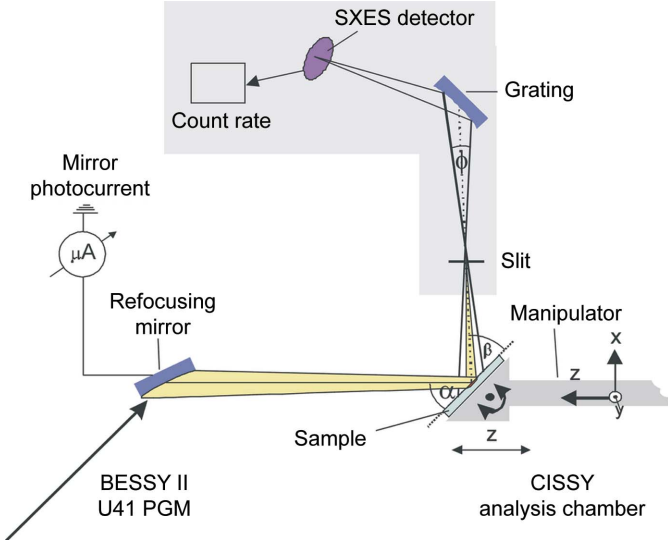

Figure 3
Set-up for SXES measurements as seen from above (*y*-direction of the manipulator). The photoelectrons emitted by the last refocusing mirror unit are detected as a direct measure of the synchrotron light intensity. In order to achieve optimal count rates the *z*-coordinate of the sample holder has to be carefully adjusted so that the synchrotron beam spot on the sample lies completely within the viewing angle of the spectrometer.

period defined by the user. The emission intensity of a particular emission line is then obtained by integrating the relevant range of the energy-dispersive spectrum. This mode offers spectral information of the peak at high resolution, for example the shape and position of the emission peak.

The second mode allows a much faster and more direct evaluation of the intensity of a particular emission line. In this mode it is necessary to tune the spectrometer (by modification of detector position and tilt) in a way that only the energy range of interest is detected by the spectrometer. Then instead of a full energy-dispersive spectrum only the integrated count rate in this range is recorded, which can then be directly used as a measure of the intensity of the particular emission line. As no high-energy resolution is required in this mode, the integration time for one single measurement is in this case reduced to the time scale of seconds.

Whereas the integration time for the first mode allows signal collection only at a fixed sample position, the second mode enables the intensity of a particular emission line to be mapped over a whole sample area (scanning mode).

3.3. Sample alignment for the spectra acquisition mode at fixed position

The sample is mounted on a fully computer-driven manipulator, which allows precise positioning with an accuracy better than 10 μm. In order to acquire an SXES spectrum at a particular spot, the sample positioning has to be optimized. According to Fig. 3, the beam spot of the synchrotron excitation on the sample needs to fall within the viewing angle of the spectrometer. In practice, this is accomplished by preselecting the desired spot on the sample by an eye-guided manipulation in the *x*- and *y*-direction (on many samples an emission in the visible range indicates the position of the incident beam on the sample). Subsequently, for a maximum SXES count rate an optimization of the *z*-position (see Fig. 3) is necessary. Since the emission intensity decreases by about 5% at a position 40 μm away from the optimal *z*-position, this optimization has to be carried out carefully for comparative emission intensity measurements to avoid errors due to misalignments. The reproducibility of SXES intensity measurements on the same sample was examined in a preliminary study. For this purpose the *z*-position for measurements on different spots was optimized independently. The standard deviation of these SXES emission intensity measurements was found to be better than 2%.

3.4. Scanning mode with moving sample and fixed energy range

On a flat co-planar sample the CISSY manipulator is able to scan the integrated SXES signal (*e.g.* the total count rate of a pre-selected energy range) over an area of up to a few mm^2. The optimal *z*-position with maximum count rate has to be found separately for the diagonally opposed start and end points of the rectangular scan area. The optimal *z*-position for any other point within the scan area is calculated by an algorithm under the assumption of a flat and co-planar sample surface. During the scan procedure the computer drives the sample holder stepwise to the next position and pauses there for a preset time while recording the integrated SXES signal. As for the spectra, during the scanning procedure the intensity of the synchrotron radiation has to be recorded for each individual measurement, for example at each individual pixel of the scan image. The integrated emission intensities are then corrected for the changing excitation conditions, as described above.

In this way lateral inhomogeneities of a sample can be monitored with a particular SXES emission over the whole scanning area. The spatial resolution of the scan is limited by the size of the beam spot, which in turn depends on the required photon flux at the sample. The different exit slits of the beamline U41-PGM allow a variation of the beam size. A compromise has to be found between high photon fluxes (with high count rates) and lower photon fluxes (with a better spatial resolution). The smallest beam spot has a size of 30 μm × 50 μm and requires very long acquisition times and a high emission intensity of the sample. For the SXES area scans reported here, basically the maximum beamline settings with a spot size of approximately 100 μm × 800 μm are chosen to keep collection times reasonable. They extend over an area of approximately 5 mm × 20 mm (10–20 min per area scan, with a collection time of the order of seconds for each spot). In practice, the overall scanning area, the number of spots, the size of the beam spot and the sampling time per spot have to be optimized for each sample separately to meet the desired signal-to-noise ratio and the desired lateral resolution. Monitoring the intensity of more than one region of interest in parallel during an area scan is not yet possible with our set-up. Therefore, for each emission line a separate scan has to be accomplished.

3.5. SXES measurements

First, S $L_{2,3}$ spectra of the bare substrates without ZnO layer were recorded as references for samples *A*, *B* and *C*. The excitation energy for all S $L_{2,3}$ measurements was 200 eV. Then, at different positions on each ZnO plateau, several SXES spectra in the fixed position spectral mode were recorded. Furthermore, a scan recording the integrated S $L_{2,3}$ emission intensity over the whole area was performed for each sample. For sample *B*, an additional complementary scan was conducted at an excitation energy of 1100 eV. This time, Zn and O emissions (Zn: $L_{2,3}M_{4,5}$; O: $KL_{2,3}$ in second-order diffraction) lay within the recorded energy region. For all SXES measurements the monitored mirror current was used to account for varying excitation conditions as described above.

4. Results

4.1. Surface roughness

The theoretical model used to estimate the impact of the surface roughness on the SXES emission intensity involved a simple rectangular saw-tooth model as outlined by Borie

(1981) for the case of X-ray diffraction intensities. The main result was that a significant decrease in emission intensity is to be expected (by a factor of ~0.8) when the surface roughness approaches the same magnitude as the involved attenuation lengths (excitation and emission).

The comparison of the measured Mo emission intensities revealed that the rough Mo sample (sample 2) yielded only 83% intensity of that of the smooth one (sample 1), which is in good agreement with the calculation. This shows that surface roughness may indeed have a significant influence on emission intensities. This fact has to be kept in mind when quantitatively evaluating SXES spectra. Only measurements on samples with similar surface roughness or a surface roughness well below the involved attenuation lengths should be compared. Under these aspects sample *A* (MoS_2/Mo/glass) can be considered as smooth. For the CIS and CIGSSe samples (*B* and *C*) the roughness probably already affects the emission intensity and therefore only samples with similar surface roughness will be directly comparable.

4.2. Comparison of S $L_{2,3}$ emission intensities of different compounds

Fig. 4 compares the S $L_{2,3}$ reference spectra of the different sulfur-containing substrates: sample *A*, MoS_2; sample *B*, $CuInS_2$; sample *C*, $Cu(In,Ga)(S,Se)_2$. Apart from changes in emission intensities the different shape of the S $L_{2,3}$ emission owing to differences in the local chemical environment of the S atoms in the different samples can be clearly seen. The 26 nm MoS_2 layer of sample *A* did not reveal a saturated sulfur S $L_{2,3}$ emission. The recorded intensity amounts to approximately 45% of the saturated emission intensity of an 'infinitely thick' MoS_2 sample (practically above 200 nm). The other two samples revealed a saturated sulfur emission owing to the rather thick sulfur-containing CIS and CIGSSe absorber layer of 2–3 µm. However, owing to the lower concentration of S atoms in the solar cell absorber materials, the saturated S $L_{2,3}$ emission intensity of these substrates still fell behind the (unsaturated) emission intensity from the MoS_2. The lowest emission intensity was found for sample *C*, the substrate with the lowest sulfur atomic content.

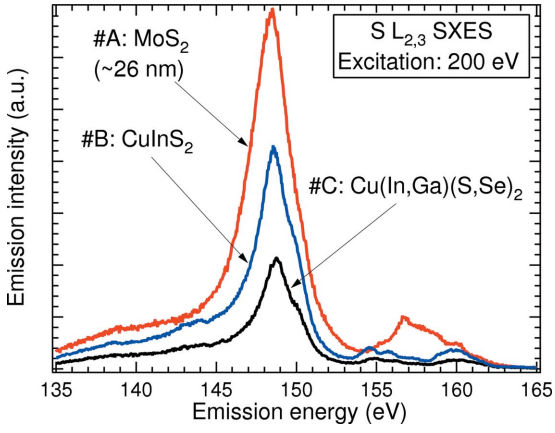

Figure 4
S $L_{2,3}$ emission spectra from the bare substrates without any ZnO cover layer for sample *A* [thin layer of MoS_2 (~26 nm), unsaturated emission], sample *B* (CIS, saturated) and sample *C* (CIGSSe, saturated). The shape of the SXES spectra is different owing to the different chemical environments of the probed S atoms in the specimen. Spectra have been corrected to standard excitation conditions. Therefore, the different specific emissivities owing to the different elemental compositions of the samples also become apparent. The ratio of the integrated emission intensities (135–165 eV) are as follows: sample *A*:sample *B*:sample *C* = 1.0:0.59:0.29.

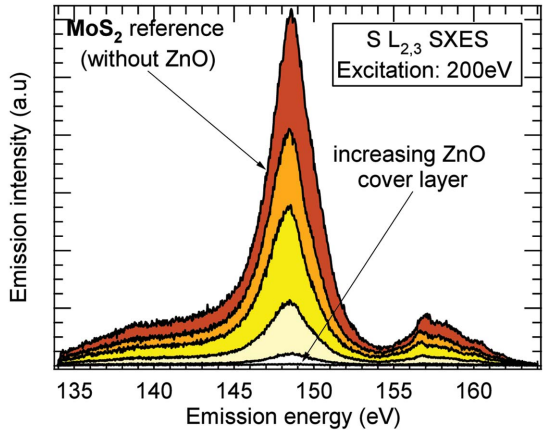

Figure 5
S $L_{2,3}$ emission spectra of MoS_2 (sample *A*) from the plain and ZnO covered areas. The recorded emission intensity decreases for increasing ZnO layer thicknesses. The spectral shape, however, remains unchanged, which illustrates that spectroscopy of buried layers is in fact possible.

4.3. Spectral mode: sample *A* (ZnO/MoS_2)

Fig. 5 shows the sulfur $L_{2,3}$ emission spectra of MoS_2 below the ZnO plateaus of different thickness on sample *A*. It should be noted that the spectral shape does not change in any significant way. The comparison of the spectra in a normalized representation (not shown) showed only slight differences owing to a decrease in the signal-to-noise ratio and an enhanced influence of the dark background.

The emission intensity in Fig. 5 decreases with increasing ZnO thickness. The integrated peak intensity was plotted *versus* the ZnO cover layer thickness as measured by ellipsometry. The data points were fitted with an exponential function and an effective attenuation length α^*_{att} [as defined in equation (3)] as fit parameter. This effective attenuation length was compared with one that has been calculated from data of the Center of X-ray Optics (CXRO) database (http://henke.lbl.gov/optical_constants/atten2.html), Lawrence Berkeley Laboratory (based on work from Henke *et al.*, 1993). The exponential fit yields for α^*_{att} a value of 12.5 nm (± 0.4 nm) which is in excellent agreement with the value of 12.9 nm extracted from the CXRO database.

4.4. Scanning mode: sample *B* ($ZnO/CuInS_2$)

The integrated emission intensity for the S $L_{2,3}$ emission line was recorded in scanning mode over the whole sample as described above. The resulting scan image is depicted in Fig. 6(*a*). In the scan the different plateaus can be clearly distinguished as steps with increasing S $L_{2,3}$ emission intensity.

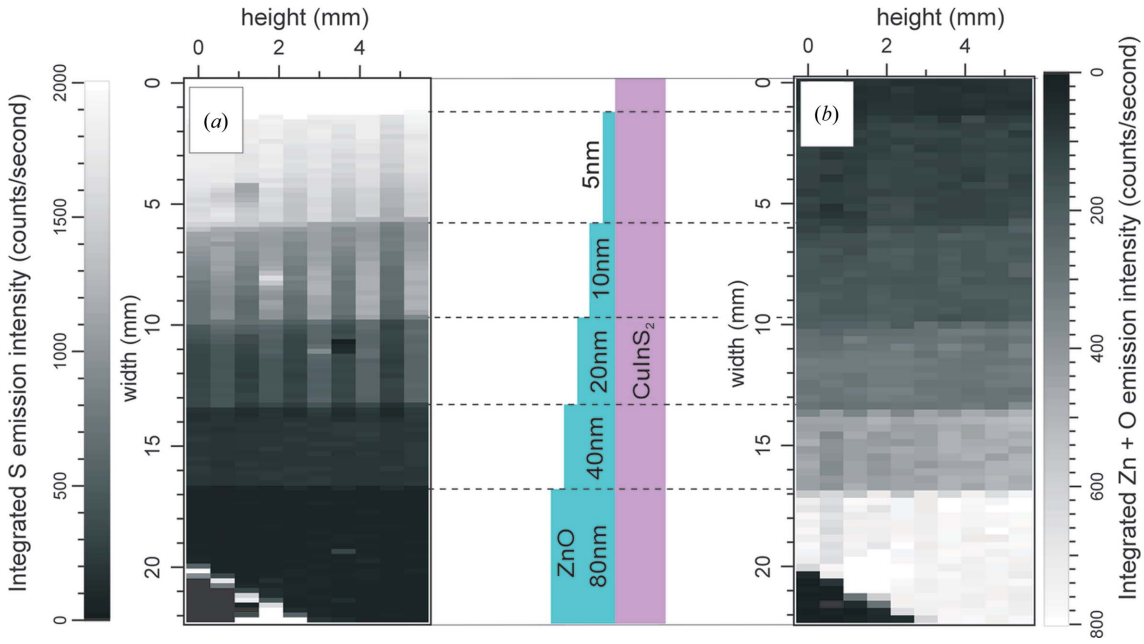

Figure 6
Two scans over the same area of sample *B* ($CuInS_2$): (*a*) SXES scan recording the integrated S $L_{2,3}$ emission and (*b*) SXES scan of the integrated Zn $M_{4,5}L_{2,3}$ and O $L_{2,3}$ emission (the O $L_{2,3}$ emission is recorded in the second diffraction order). The stepwise increase of the ZnO-layer thickness is clearly resolved in the scan images as (*a*) decreasing and (*b*) increasing emission intensity of the corresponding signals (bright = high intensity).

The brightness modulation of every second line, however, is an artefact of the scanning procedure, since the scanning direction is reversed at the end of each line scan and a minute slip of the manipulator leads to a slightly different sample position away from the optimum alignment. This shortcoming may be improved in future scan measurements by simply changing the scanning procedure to scan each line in the same direction. In the case of the particular scan image discussed here, only data points of every second line (forward direction) were taken into account in the coming quantitative discussion. All data points within one plateau were averaged and the emission intensities were evaluated according to the considerations outlined in §2.

Fig. 6(*b*) shows the complementary scan image of the same sample, this time recording the Zn and O emission lines. Again, the steps in the ZnO structure can be clearly observed. In contrast to the S $L_{2,3}$ scan where an attenuation of the emission intensity is observed, this time an increasing emission intensity reflects the increasing ZnO layer thickness. Scans of the second type can be used for the determination of layer thicknesses by the evaluation of the unsaturated signal of a thin emitting layer as developed in §2 [equation (4)].

The graphs in Fig. 7 show the intensity of the S $L_{2,3}$ and Zn $L_{2,3}M_{4,5}$ fluorescence lines as a function of the thickness of the ZnO layer. As is the case for sample *A*, the relative S $L_{2,3}$ emission intensity falls exponentially with an increasing *absorbing* ZnO layer (see Fig. 6*a*). Here, the attenuation of the signal in the cover layer can be used to determine its thickness. In contrast to this the combined Zn and O emission intensities are increasing as the *emitting* ZnO layer becomes thicker until

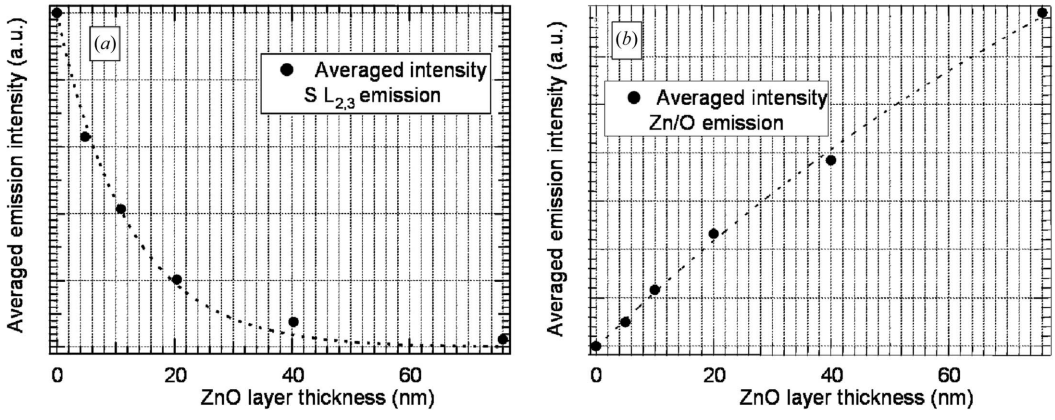

Figure 7
SXES emission intensities averaged over the ZnO plateaus from sample *B* (CIS) are plotted *versus* the ZnO layer thickness of the corresponding plateaus. The dotted lines are exponential fits to the experimental data. (*a*) The averaged S $L_{2,3}$ emission intensity of the scan image in Fig. 6(*a*). (*b*) The averaged combined Zn/O emission intensity of the scan image shown in Fig. 6(*b*).

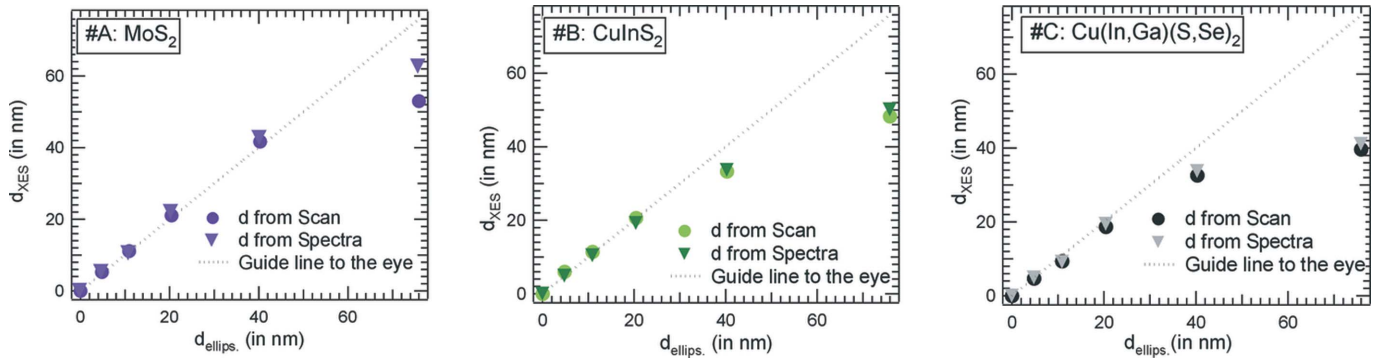

Figure 8
Graphical representation of the calculated ZnO layer thicknesses for the different plateaus and different samples. For comparison, the calculated ZnO layer thickness *d* as obtained from the measured SXES emission intensities is plotted against the ellipsometrically measured layer thickness for all samples and plateaus. The results obtained from the averaged relative emission intensities of the scan measurements are in good agreement with the results from the local spot measurements. Additional (grey) background radiation can significantly alter the calculated ZnO layer thickness for low SXES emission intensities (thick absorbing ZnO layers), resulting in lower calculated layer thicknesses. This effect can clearly be seen in all samples for a layer thickness of 80 nm ZnO.

a saturation limit is reached. However, in this particular case the emission intensity of the thickest cover layer is still far away from the saturation (see Fig. 6*b*). Theoretically, the Zn $L_{2,3}M_{4,5}$ emission intensity from a ZnO layer should reach 99% of the saturation value at a layer thickness of about 600 nm. Consequently the almost linear dependency of the emission intensity on the thickness can be used as well to determine the cover layer thicknesses. The complementary determination of the cover layer thickness by evaluation of the absorption of the substrate signal and the separate evaluation of a (different) emission signal of the cover layer yields most accurate results.

4.5. Sample *C* (ZnO/CIGSSe)

The results for the CIGSSe absorber (sample *C*) followed closely those obtained from the other two samples and are compared with the others in the following section.

5. Discussion

The relative S $L_{2,3}$ emission intensities of the different plateaus were evaluated in terms of a cover layer thickness (of ZnO) using the standard absorption law (as outlined in §2). In Fig. 8 the experimentally determined ZnO layer thicknesses by the three SXES series are plotted *versus* the thickness measured by ellipsometry.

Up to 40 nm the calculated layer thickness correlates very well with the results obtained by ellipsometry. However, for the plateau with a ZnO thickness of 76 nm the measured net S $L_{2,3}$ emission intensities were significantly higher than expected and resulted in significantly lower calculated thicknesses (*e.g.* 63 nm for the spot measurement sample *A*). This effect can be understood by considering the rather low overall count rate of approximately 90 counts s^{-1} observed at a ZnO thickness of 76 nm. At the time of the experiment the detector showed a typical dark count rate of about 32 counts s^{-1} (without any sample and synchrotron excitation present). This background is automatically subtracted from all spectra after each measurement. Responsible for the deviation at low count rate is any additional non-specific background radiation stimulated by the incident synchrotron radiation ('grey background'), *e.g.* inelastic scattering in the ZnO layer. This grey background adds to the measured net S $L_{2,3}$ emission intensity. At low count rates (corresponding to thick ZnO layers) the contribution of the grey background may significantly increase the measured signal intensity. A precise quantification of the grey background is not yet satisfactory. It requires reference samples similar to the samples used in this experiment with the only difference that any contribution of the substrate to the S $L_{2,3}$ emission intensity can be excluded. Difficulties arise owing to the fact that proper sample alignment is then almost impossible. However, practice shows that if plain ZnO is excited by the synchrotron beam (200 eV) there is a non-zero contribution (at least 5–10 counts s^{-1}) which is different from any known S $L_{2,3}$ emission. As soon as the count rate approaches the magnitude of the grey background, the quantification limit of the method is reached.

6. Summary and conclusion

This paper demonstrates the potential of quantitative SXES analysis. It follows the standard evaluation techniques for quantitative XRF analysis in terms of layer thickness and/or elemental composition and extends them to the soft X-ray regime (energy range 100–1500 eV). The information depth for SXES of up to a few hundred nanometres is ideally suited to probe thin films and even buried interfaces and to complement, for example, more surface-sensitive X-ray photoelectron spectroscopy measurements. The major advantage of SXES over XRF is the possibility to probe the local chemical environment of the specific elements, which for example means that chemical changes at interfaces can be detected. This advantage is not affected by cover layers as long as the emission of the bottom layer does not interfere with an emission of a cover layer. In these cases it is possible to

evaluate the SXES signals quantitatively. It was found in our work that Beer's law of X-ray attenuation is applicable without any modifications, and mass absorption coefficients currently available in the CXRO database yield meaningful results. In turn, the attenuation of signals by a cover layer could be used to quantify the cover layer thickness itself.

The limits of such a quantification approach were explored for model systems with ZnO on top of different sulfur-containing substrates. As soon as the count rate approaches the order of background radiation the quantification becomes inaccurate. A grey background, inelastic transitions in the same energy range, leads to an additional signal and an overestimation of the actual SXES emission. However, for sufficiently high SXES count rates the strength of the method lies in the accurate determination of the thickness of very thin cover layers even on rough polycrystalline surfaces.

A quantification of film thickness on rough surfaces is usually very difficult and so the monitoring of SXES signals, particularly of lighter elements, provides a powerful new method. The surface roughness itself has a significant impact on measured emission intensities as soon as the attenuation length approaches the magnitude of the surface roughness. Usually it is sufficient to ensure that only the emission signals of samples of similar surface roughness are compared.

In addition, we demonstrated that SXES emission intensities at different spots with an overall lateral resolution of 50–100 μm and better can be recorded. With an automated scanning mode the integrated SXES emission intensity within a pre-selected energy range can be collected over a whole area pixel by pixel. With this method an evaluation of thin films and buried interfaces can be accomplished easily over an area of several millimetres and lateral inhomogeneities can be visualized.

We would like to thank Professor Dr Clemens Heske, University of Nevada Los Vegas, for sharing his knowledge on soft X-ray emission spectroscopy and fruitful scientific discussions. Avancis GmbH & Co KG (formerly Shell Solar GmbH, Munich, Germany) are gratefully acknowledged for providing $Cu(In,Ga)(S,Se)_2$ absorbers.

References

Borie, B. (1981). *J. Appl. Cryst.* **14**, 219–222.
Henke, B. L., Gullikson, E. M. & Davis, J. C. (1993). *Atom. Data Nucl. Data Tables*, **54**, 181–342.
Heske, C. *et al.* (1999). *Appl. Phys. Lett.* **74**, 1451–1453.
Heske, C., Groh, U., Fuchs, O., Weinhardt, L., Umbach, E., Grün, M., Petillon, S., Dinger, A., Klingshirn, C., Szuszkiewicz, W. & Fleszar, A. (2003). *Appl. Phys. Lett.* **83**, 2360–2362.
Jenkins, R., Gould, R. W. & Gedcke, D. (1981). *Quantitative X-ray Spectroscopy*, 1st ed. New York/Basel: Marcel Dekker.
Jung, C., Eggenstein, F., Hartlaub, S., Follath, R., Schmidt, J. S., Senf, F., Weiss, M. R., Zeschke, Th. & Gudat, W. (2001). *Nucl. Instrum. Methods Phys. Res. A*, **467–468**, 485–487.
Klaer, J., Luck, I., Boden, A., Klenk, R., Gavilanes Perez, I. & Scheer, R. (2003). *Thin Solid Films*, **431–432**, 534–537.
Kötschau, I. M., Weber, A., Pistor, P., Lauermann, I., Fischer, Ch.-H. & Schock, H. W. (2007). *Thin Solid Films*, **515**, 5992–5996.
Mönig, H., Lauermann, I., Grimm, A., Camus, C., Kaufmann, C. A., Pistor, P., Jung, Ch., Kropp, T., Lux-Steiner, M. C. & Fischer, Ch.-H. (2008). *Appl. Surf. Sci.* **255**, 2474–2477.
Nordgren, J. & Guo, J. (2000). *J. Electron Spectrosc. Relat. Phenom.* **110–111**, 1–13.
Rusu, M., Bär, M., Lehmann, S., Sadewasser, S., Weinhardt, L., Kaufmann, C. A., Strub, E., Röhrich, J., Bohne, W., Lauermann, I., Jung, Ch., Heske, C. & Lux-Steiner, M. Ch. (2009). *Appl. Phys. Lett.* **95**, 173502.
Tertian, R. & Claissse, F. (1982). *Principles of Quantitative X-ray Fluorescence Analysis.* London/Philadelphia/Rheine: Heyden.
Weinhardt, L., Blum, M., Bär, M., Heske, C., Fuchs, O., Umbach, E., Denlinger, J. D., Ramanathan, K. & Noufi, R. (2007). *Thin Solid Films*, **515**, 6119–6122.